Molecular Dynamics Simulation: the Effect of Graphene on the Mechanical Properties of Epoxy Based Photoresist: SU8

Faraz Mohammadzadeh Honarvar [a], Behzad Pourabbas [a,*], Mehdi Salami Hosseini [a],

Mahsa Kharazi [b], Hamid Erfan-Niya [c]

a) Department of Polymer Engineering, Nanostructured Materials Research Centre, Sahand University of Technology, Sahand New Town, Tabriz, Iran.

b) Department of Mechanical Engineering, Sahand University of Technology, Sahand New Town, Tabriz, Iran.

c) Department of Chemical and Petroleum Engineering, University of Tabriz, Tabriz, Iran

*) Corresponding author: Email: pourabas@sut.ac.ir, Tel: +98 41 3344 9083, Fax: +98 41 3344 4303, mobile: +98 914 112 0916

E-mail addresses of authors:

Faraz Mohammadzadeh Honarvar: f_mohamadzadeh@sut.ac.ir

Mehdi Salami Hosseini: salami@sut.ac.ir

Mahsa Kharazi: kharazi@sut.ac.ir

Hamid Erfan-Niya: herfan@tabrizu.ac.ir

Abstract

SU8 is an epoxy-Novolac resin, which is used as photo initiator in micro- and nano- fabrication techniques. From literature, graphene has been proved that results in significant improvement in the properties of the composites. However, due to nanometer size of the graphene layers there is no any experimental tool to obtain insight of the fillers inside the resin especially when the materials are under mechanical deformations where simulation techniques work well. Therefore, SU8 and SU8-graphene nanocomposites as the model compounds were taken to be investigated from atomistic molecular dynamic approach to demonstrate the effect of graphene layers. This leads to mechanical property enhancement such as Young's, bulk and shear modules being affected by the aspect ratio of the graphene layers high aspect ratio graphene in SU8 leads to an 81% improvement in Young's, 100% in bulk and 83% in shear moduli in addition to higher density and less graphene wrinkling.

Keywords: SU8; Graphene; Nanocomposite; Mechanical properties; Molecular dynamics

1. Introduction

The resin with the commercial name SU8 is an epoxy-Novolac resin is used mainly as a negative sub-micron resolution photoresist in lithographic processes. The properties of SU8, such as rigidity, low toxicity, transparency to visible light, high thermal and chemical stability, low cost and simplicity of the process, has led to a broad range of applications in micro- and nano-fabrications. Sensors, micro lenses, optical devices, etched resist masks, micro fluidics, microelectromechanical systems (MEMS) are just examples of many devices in which SU8 can be used in one or more steps of production [1-9].

Recently, researches have been able to alternate the properties of nano-filled polymers (electrical, optical, thermal, mechanical, rheological, barrier etc.) by using different available

nano-sized particles (NPs) as the filler. As the matter of fact, only a few weight percent of the fillers, in contrast to traditional composites, is enough for a large improvement in the properties [10-13]. Nanoclays, silica nanoparticles, carbon nanotubes (CNTs) and other carbon based particles including diamantens and single-layer graphene layers are amongst the widely used NPs used for newly developed materials and nanocomposites [14-17]. Though outstanding properties are reported for graphene-polymer nanocomposites [11,18,19] however, from experimental point of view, there is not any instrumental method to investigate the real stories of the nanomometric scale interactions of the materials remaining as a big challenge. Though many experimental methods have been developed to probe at the finer scale of the materials however, the knowledge, undoubtedly, is necessary to the engineers to design new materials with desired properties without exceeded number of the experimental trials [20]. To this purpose, graphene in polymeric nanocomposites have been subjected by several theoretical studies using molecular dynamics (MD) simulation techniques [21-25]. This is indeed the hierarchical approach of the simulation or multiscale simulation hypothesis, which describes how the macroscale properties can be predicted based on the data from the shorter scale of the lengths i.e. the molecular dynamics. For instance, atomistic MD simulation was employed by Skountzos et al. for graphene in PMMA in order to correlate the experimentally measured macro mechanical properties of the material to the atomistic scale interactions between the polymeric matrix and the filler [26]. Functionalized graphene added to PMMA at very low content, was showed that could lead to very strong multifunctional material.

Multi-scale simulation concept was used by Ebrahimi et al. to compare how graphene or carbon nanotube are effective on the mechanical properties of Chitosan based materials with the results showing that graphene reinforcing effect being higher than that of carbon nanotubes [27].

Graphene-epoxy nanocomposites were studied by Rahman and Haque in order to estimate the elastic constants using MD and molecular mechanic (MM) simulation methods. The methodology was proven that compared to Mori-Tanaka model, the results are in better fitting with the experimental data [28].

The method developed by Theodorou et al. and Rapold et al. provides the basic calculation and the methodology for correlating and connectivity between the molecular scale interactions to the macroscale properties in polymeric materials [29,30]. According to this method, the system under simulation is subjected to a series of small strain deformations. Subsequently the elastic constants are theoretically estimated from the second derivative of internal energy (U) with respect to imposed strain. The method employed on atactic polypropylene showed acceptable results with the experimental data [31].

For the first time SU8 and SU8-graphene nanocomposites are being studied in the present work using Theodorou et al. and Rapold et al. method. This involves several MD simulation and mathematical steps leading to realistic description of the interactions between the molecules of the components leading to prediction of the macroscale mechanical properties. The simulation details and the calculations toward the mechanical property determination are provided in the following sections in addition to graphical and numerical results.

2. Simulation details

The commercial SU8 is a single component product, which consists of a multifunctional epoxy-Novolac resin, γ-butyrolactone as the reactive diluent and a photoinitiator [32-34]. For the cured product, different densities have been reported varying from 1.05 to 1.19 g/cm^3 depending to the process conditions and composition [35-38]. From structural point of view, the cured SU8 is a

real three dimensional network and therefore, the key point in MD simulation, is to find a substituted but smaller structure to represent the real compound's properties. This was carried out by examining several suggested molecular structures using previously published works on the structural analysis of the cured SU8. In order to do this, results obtained by Jun Zhang et al. on the structural analysis of the cured SU8 and MD simulation done by Lik-ho Tam et al. were considered [32,38]. Jun Zhang et al., fragmented the completely cured SU8 inside a mass spectrometer in order to depict a chemical structural for the cured SU8 network and determined the different chemical fragments with population percent. On the other hand, Lik-ho Tam simulated the cross-linking of SU8 using an effective dynamic algorithm under pcff, cvff and dreiding force fields. Ring opening polymerization without termination was the polymerization reaction which was considered for curing simulation. For the terminal atoms, hydrogens were substituted to achieve saturation of the bonds. The final degree of cross-linking and density using pcff force field were achieved to be 82.5% and 1.053 g/cm^3, respectively. Therefore, several structures were assembled and energy minimization process was performed for all of the suggested structures using pcff force field with 8 A□ cutoff distance at room temperature (298 °K) until the total potential energy of each system was reached to its minimum state. The structure with the comparatively lowest potential energy was selected to be the representative structure for SU8 and was used in MD simulation procedure. The representative structure is shown in Figs.1a and b, which is consisted of the main structure of the original SU8 as the core, two free epoxy groups and six epoxy groups reacted with γ-butyrolactone in a specific manner in order to resemble the cured SU8 as the model compound for simulation.

For the nanocomposites, two types of graphenes with different aspect ratios were embedded in the simulation box including a high aspect ratio graphene (GH) (layer dimensions: of 26.18 A□

× 13.337 A□) and low aspect ratio graphene (GL) (layer dimensions: 19.638 A□ × 14.546 A□) as are shown in Figs. 1b and c, respectively.

Five model compounds were simulated for MD and mechnical property calculations. These are including a simulation cell consisting of 50 model SU8 without graphene, 50 model SU8 with one or two high aspect ratio graphene, 50 model SU8 with one or two low aspect ratio graphene. Thus, taking all of the atoms in the simulation cell, the weight percent of the garphene (low and high aspect ratios) in SU8/graphene nanocomposites are 2.1 or 4.2 wt.% (weight percent) depending to the number of graphene layeres in the simulation cell. Table 1 summarizes the detailed constituents of each simulated compound while Fig.2 shows the snapshot for the simulation cell for SU8-GH42.

The simulation procedure was performed on the simulation cell with periodic boundary conditions in all dimensions and pcff force field was employed to compute the atomic interactions within a cutoff distance of 8 A□. In order to bring the system to the conformational stability, simulation cells were subjected to 100000 steps of energy minimization followed by MD runs under isobaric isothermal ensemble (NPT) without applying any external pressure at 298 °K. This was continued until the system is reached to the equilibrated state of energy, temperature and density. The temperature and pressure were controlled by Nosé-Hoover thermostat-barostat algorithm [39,40]. For further equilibration, an isothermal isochoric ensemble (NVT) was performed on the system at 298 °K. The system was analyzed for its energy, structure and dynamics after the system had been reached to the new equilibrated state. The MD runs were performed for 2×10^6 steps of 0.1 fs and differential equations of motion were integrated using the velocity Verlet integrator [41,42] during the simulation run. Finally, the mechanical properties of SU8 and its nanocomposites were calculated based on the procedure

previously developed by Theodorou [29]. Open source code LAMMPS was used in all of the MD simulation steps described above [43].

The procedure for the mechanical property calculation and prediction was as follow:

1- First, for the optimized configurations obtained from the previous MD runs energy minimization was performed once again to ensure the optimum geometry and minimum energy.
2- Applying strains (less than 1%).
3- Reoptimizing of the potential energy of the resulting structure.
4- Repeating steps 1 to 3 on the next optimized configuration from the MD run.
5- Averaging the mechanical properties over the data obtained for each configuration described above.

The elastic constants are calculated from the second derivative of internal energy (U) with respect to the imposed strain according to Eq.1.

$$C_{ij} = \frac{1}{V} \frac{\partial^2 U}{\partial \varepsilon_i \partial \varepsilon_j} = \frac{\partial \sigma_i}{\partial \varepsilon_j} \quad \textbf{(Eq. 1)}$$

Lame constants (λ, μ) can be obtained from the elastic constants using Eqs. 2 and 3.

$$\lambda = \frac{1}{3}\left(C_{11} + C_{22} + C_{33}\right) - \frac{2}{3}\left(C_{44} + C_{55} + C_{66}\right) \quad \textbf{(Eq. 2)}$$

$$\mu = \frac{1}{3}\left(C_{44} + C_{55} + C_{66}\right) \quad \textbf{(Eq. 3)}$$

Now, the mechanical properties can be derived from the obtained Lame constants (Eqs. 4 to 6):

$$E = \mu \frac{3\lambda + 2\mu}{\lambda + \mu} \quad \textbf{(Eq. 4)}$$

$$B = \lambda + \frac{2}{3}\mu \quad \textbf{(Eq. 5)}$$

$$G = \mu \quad \textbf{(Eq. 6)}$$

Detailed formulations and calculations are available in the literature [26,29].

3. Results and discussions

3.1. Structural properties

According to the procedures described above, the average density of the SU8 and SU8/Graphene nanocompistes were calculated and are summarized in Table 2.

A range of experimental and theoritical values are reported in the literature for SU8 from 1.05 to 1.19 g/cm^3 [35-37]. Therefore, the predicted value for the pure SU8 which is indeed, based on the model SU8 structure supposed in this work, 1.108 ± 0.002 g/cm^3 an acceptable agreement is seen. However, the predicted density for the nanocomposites with high aspect ratio graphene is seen to be slightly higher than that of pure SU8 while the nanocomposites with low aspect ratio graphene show lower densities. This obviously, is related to the SU8 packing around the high

aspect ratio graphene layers leading to the denser packing of the materials in the simulated nanocomposite systems. Inversely, in the case of the low aspect ratio graphene layers, orientation and packing of the SU8 molecules results in lower density of the materials around the layers. This of course, can be verified by the radius of gyration R_g and end-to-end distance of the SU8 molecules in the simulated systems. The R_g versus probability density of the model SU8 is plotted in Fig. 3 and the numerical values are reported in Table 3. It can be seen that graphene lowers R_g of the model SU8 molecules with respect to the pure SU8 however; this depends on the aspect ratio of the graphene layers in the system. The calculated R_g for the GL nanocomposites is 9.70 or 9.31 Å while this is 8.81 or 9.01 Å for the GH nanocomposites. Keeping R_g value of the pure SU8 as the reference point 10.42 Å, lower R_g can be regarded as an indication of higher intramolecular interactions (or lower intermolecular interactions) with respect to the reference configuration (the pure SU8). In conclusion, high aspect ratio graphene prevents intermolecular interactions between SU8 molecules in a greater extent than the low aspect graphene does. This can, of course, lead to two major conclusions. Firstly, any intermolecular interactions between graphene and SU8 are not a subject. Secondly, graphene imposes its effect through surface area as, high aspect ratio has greater surface area (698.325 $Å^2$) than low aspect (570.600 $Å^2$).

A useful results obtained from the MD simulation is the radial distribution function (RDF) or element pair distribution functions which provides detailed information about the local packing and structural distribution over the length scale. The intramolecular pair distribution reflects intramolecular forces between the paired atoms belonging to the same molecule and intermolecular pairs in the same manner, is the reflection of the interactions between atoms from

different molecules. The RDF plots for atoms in the model SU8 for pure and the nanocomposites are shown in Figs. 4 and 5.

In Figs. 4 and 5, the function $g_{\alpha\text{-}\beta}(r)$ is the length scale dependent contribution function showing atom α being in interaction with atom β both belonging either to the same molecule (intramolecular) or different molecules (intermolecular). For the intermolecular interaction in Fig 4, $g_{\alpha\text{-}\beta}(r)$ approaches 1 at long distances obviously, because all the paired interactions lay within the sphere of infinite radius. However, $g_{\alpha\text{-}\beta}(r)$ for intramolecular distribution in Fig. 5, reaches zero at long distance because atomic distribution for the atoms in a single molecule lay in a sphere with certain volume. The function $g_{\alpha\text{-}\beta}(r)$ however, follows almost the same pattern for the pure SU8 and the nanocomposites especially in the case of the intramolecular distribution and shorter distances (Fig. 5). The sharp hump or depression regions are indeed, determined by the configurationally limitations including bond distance, angular rotations, temperature and so on. If $g_{\alpha\text{-}\beta}(r)$ is compared, for instance $g_{C\text{-}C}(r)$, for inter and intramolecular distribution, it can be concluded that the $g_{\alpha\text{-}\beta}(r)$ values are different for different compound, SU8 and the nanocomposites, at a certain distance. Due to phenomenological properties of $g_{\alpha\text{-}\beta}(r)$, this can be attributed to different intermolecular and intramolecular distributions in the specimens. As an example, $g_{C\text{-}C}(r)$ of the intermolecular distribution (Fig. 4) shows lower values for SU8-GL42 compared to pure SU8 all over the length scales. This is while $g_{C\text{-}C}(r)$ of the intramolecular distribution (Fig. 5) for the same nanocomposite shows higher values with respect to the pure SU8. Therefore, knowing the fact that intermolecular or intramolecular interactions are balanced in the most stable configuration, the paired atomic distribution function can be regarded as the function that provides information about the configuration and that how it is comparable at

different conditions. In other words, lower interamolecular distribution deals with comparatively less effective intermolecular interactions or higher intramolecular interactions. The balanced intra- and intermolecular interactions build the most stable configuration for the chain resulting in a characteristic R_g. Therefore, from the data in Table 3, the reason for reduced R_g of the nanocomposites with respect to the pure SU8 can be related to the graphene layer which indeed, reduces the intermolecular interactions of the SU8 molecules. Graphene layers apply this shielding effect through the surface so that high aspect ratio graphenes with higher surface area show comparatively lower R_g (Table 3). Additionally, in Fig. 5, absence of any periodical sharp peaks at distances greater than 4 Å and tending RDF to 1 provide proofs for the system being in amorphous morphology.

3.2. Graphene orientation

One major effect of intermolecular interactions or tensile loads is the graphene deformation from its originally flat structure to a wrinkled or deformed state. It has been studied in several new works by molecular simulation techniques [44,45]. Planner atomic distribution profile is a tool that helps to understand where the graphene is located, what is the orientation and that how the graphene is deformed inside the simulation cell. Fig. 6 illustrates the relative atomic concentration planner profile along the three main simulation axis (001, 010, 001) for the nanocomposite containing 2.1 wt.% of GH or GL graphene, just after molecular stabilization and before any applied deformation load. Whether the graphene is high or low aspect one, location, orientation and deformation will be different as is clear on the concentration profiles and in snapshots given for each nanocomposite shown in Fig. 6. High aspect graphene in SU8-

GH21 is lying supine alongside ‘x’ axes (100 plane) facing up toward ‘y’ axes (010 plane). This is while graphene in SU8-GL21 is almost is standing alongside ‘y’ axes facing almost to ‘z’ direction (001 plane). Though these are random positions, which can happen in any other conformation by successive MD simulations however, the most important concern with the graphene layer within the nanocomposite is wrinkling or deformation. Relative atomic concentration shows plateau humps for high aspect graphene in SU8-GH21 that is appeared as sawtooth mark in SU8-GL21 providing a proof that the low aspect graphene is wrinkled alongside of the all three axis of simulation cell. This of course, will affect the mechanical properties of the nanocompoaites, which is being discussed in later section.

3.3. Mechanical properties

Mechanical properties of the simulated systems were predicted based on the methodology described earlier in section 2. A constant strain was applied to the pure SU8 and to the nanocomposites. Any structural symmetry was removed from the system and then re-optimized, if necessary, to the lowest energy level. At the end of the process, the mechanical properties were calculated by avaraging the quantitative parameters as described earlier. The normalized calculated mechanical properties (Young, shear and bulk modulus) are listed in Table 4.

Data in Table 4 is also compared graphically in Figs. 7 to 9. As the first conclusion, incorporating graphene in SU8 enhances the mechanical properties of the nanocomposites with respect to the pure SU8. For instance, Young, bulk and shear modulus in SU8-GH21 are increased to 63%, 202% and 82% respectively, with respect to pure SU8. Moreover, due to the increased weight percent of graphene in SU8-GH42 the mechanical properties can be seen that are more increased to 81%, 216% and 83%, respectively.

However, high aspect ratio graphene in the nanocomposites show higher reinforcement effect as is clear in Table 4 or comparative graphical demonstrations in Figs. 7 to 9. This can be related to the density of the nanocomposites given in the preceding sections based on the density of the nanocomposites and being dependent to the aspect ratio of the graphene. In other words, relatively lower moduli for the compounds with low aspect ratio graphene, in SU8-GL21 and SU8-GL42, is due to the lower materials packing or lower density of the compounds. For instance, if the bulk modulus is concerned, it is a reflection of how the materials are compressible or how much the density of the material decreases (dρ) in effect of an applied infinitesimal pressure (dP) described mathematically as Eq. 7.

$$B = -V \times \left(\frac{\partial P}{\partial V}\right)_T \qquad \text{Eq. (7)}$$

or, in terms of density change:

$$B = \rho \times \left(\frac{\partial P}{\partial \rho}\right)_T \qquad \text{Eq. (8)}$$

Accordingly, the inverse of the bulk modulus is called the compressibility, β:

$$\beta = \frac{1}{B} \qquad \text{Eq. (9)}$$

The bulk compression involves only short-range conformational changes whereas shear and tensile forces can cause strong (time-dependent) long-range conformational changes. Hence, the bulk modulus is the only time-independent modulus being a linear elastic property rather than viscoelastic one [46].

Therefore, the materials density is implicated in the bulk modulus of the nancompsites: if the the bulk moldulus of the SU8-GL nanocomposites is lower than that of SU8-GH nanocomposites (Table 4, Fig. 8) they are easily compressable compared to SU8-GH nanocompoistes due to less materials packing or lower density showing lower relative mechanical properties expectedly.

Graphene deformation and wrinkling, discussed based on relative concentration profiles in the previous section, is also provides that wrinkled graphene layer, will of course, show lower mechanical reinforcement effect due to reduced interfacial interactions with the surrounding polymer.

4. Conclusion

In this work, the atomistic molecular dynamics (MD) simulation was used to simulate SU8 epoxy resin and its nanocomposites with graphene in order to investigate the effect of graphene on the mechanical properties of SU8. Two types of graphene layers were considered to determine the influence of graphene aspect ratio. The interactions in simulated systems were calculated using LJ potential with cutoff distance equal to 8 Å and all simulation boxes had periodic boundary conditions in all directions. After energy minimization, the system was subjected to several steps of NPT run followed by several steps of NVT run at room temperature for equilibration and to collect the required data. Data showed that the low aspect ratio graphene has a negative effect on the materials packing leading to lower density. The mechanical properties estimated based on constant strain approach elucidated that the high aspect ratio graphene leads to higher mechanical properties of the nanocomposites as a direct effect of higher density. Graphene wrinkling was observed in low aspect ratio containing nanocomposites which of course, is an endorsement for the observed lower mechanical properties.

5. Acknowledgment

The authors wish to express their gratefulness from Iran Nanotechnology Initiative Council for their partial financial support of the work under contract no. of 71734. Also make their expression of thank for the research and technology affair of the Sahand University of Technology which the work has been successfully accomplished due to their supports.

6. References

1. Blagoi, G., Keller, S., Persson, F., Boisen, A. and Jakobsen, M.H. "Photochemical modification and patterning of SU-8 using anthraquinone photolinkers", *Langmuir*, **24** (18), pp. 9929-9932 (2008).

2. Hu, M., Guo, Q., Zhang, T., Zhou, S. and Yang, J. "SU-8-Induced Strong Bonding of Polymer Ligands to Flexible Substrates via in Situ Cross-Linked Reaction for Improved Surface Metallization and Fast Fabrication of High-Quality Flexible Circuits", *ACS Appl. Mater. Inter.*, **8** (7), pp. 4280-4286 (2016).

3. Nagaiyanallur, V.V., Kumar, D., Rossi, A., Zu□rcher, S. and Spencer, N.D. "Tailoring SU-8 Surfaces: covalent attachment of polymers by means of nitrene insertion", *Langmuir*, **30** (33), pp. 10107-10111 (2014).

4. Rahiminejad, S., Pucci, E., Haasl, S. and Enoksson, P. "SU8 ridge-gap waveguide resonator", *Int. J. Microw. Wirel. T.*, **6** (05), pp. 459-465 (2014).

5. Rodríguez-Ruiz, I., Llobera, A., Vila-Planas, J., Johnson, D.W., Gómez-Morales, J. and García-Ruiz, J.M. "Analysis of the structural integrity of SU-8-based optofluidic systems for small-molecule crystallization studies", *Anal. Chem.*, **85** (20), pp. 9678-9685 (2013).

6. Romeo, A., Liu, Q., Suo, Z. and Lacour, S.P. “Elastomeric substrates with embedded stiff platforms for stretchable electronics”, *Appl. Phys. Lett.*, **102** (13), pp. 131904 (2013).

7. Tian, Y., Shang, X., Wang, Y. and Lancaster, M.J. “Investigation of SU8 as a structural material for fabricating passive millimeter-wave and terahertz components”, *J. Micro/Nanolithogr. MEMS. MOEMS.*, **14** (4), pp. 044507-044507-9 (2015).

8. Feng, R. and Farris, R. “The characterization of thermal and elastic constants for an epoxy photoresist SU8 coating” *J. Mater. Sci.*, **37** (22), pp. 4793-4799 (2002).

9. Mehboudi, A and Yeom, J. “A two-step sealing-and-reinforcement SU8 bonding paradigm for the fabrication of shallow microchannels”. *J. Micromech. Microeng.*. **28** (3), pp. 035002 (2018).

10. Ramanathan, T., Stankovich, S., Dikin, D., Liu, H., Shen, H., Nguyen, S. and Brinson, L. “Graphitic nanofillers in PMMA nanocomposites—an investigation of particle size and dispersion and their influence on nanocomposite properties”, *J. Polym. Sci. Poly. Phys.*, **45** (15), pp. 2097-2112 (2007).

11. Ramanathan, T., Abdala, A., Stankovich, S., Dikin, D., Herrera-Alonso, M., Piner, R., Adamson, D., Schniepp, H., Chen, X. and Ruoff, R. “Functionalized graphene sheets for polymer nanocomposites”, *Nat. Nanotechnol.*, **3** (6), pp. 327-331 (2008).

12. George, J.J. and Bhowmick, A.K. “Ethylene vinyl acetate/expanded graphite nanocomposites by solution intercalation: preparation, characterization and properties”, *J. Mater. Sci.*, **43** (2), pp. 702-708 (2008).

13. Villar-Rodil, S., Paredes, J.I., Martínez-Alonso, A. and Tascón, J.M. “Preparation of graphene dispersions and graphene-polymer composites in organic media”, *J. Mater. Chem.*, **19** (22), pp. 3591-3593 (2009).

14. Duplock, E.J., Scheffler, M. and Lindan, P.J. “Hallmark of perfect graphene”, *Phys. Rev. Lett.*, **92** (22), pp.225502 (2004).

15. Schniepp, H.C., Li, J-L., McAllister, M.J., Sai, H., Herrera-Alonso, M., Adamson, D.H., Prud'homme, R.K., Car, R., Saville, D.A. and Aksay, I.A. “Functionalized single graphene sheets derived from splitting graphite oxide”, *J. Phys. Chem. B*, **110** (17), pp. 8535-8539 (2006).

16. Geim, A.K. and Novoselov, K.S. “The rise of graphene”, *Nat. Mater.*, **6** (3), pp. 183-191 (2007).

17. Szatkowski, P., Pielichowska, K. and Blazewicz, S. “Mechanical and thermal properties of carbon-nanotube-reinforced self-healing polyurethanes”, *J. Mater. Sci,*. **52** (20), pp. 1-14 (2017).

18. Cai, D. and Song, M. “Recent advance in functionalized graphene/polymer nanocomposites”, *J. Mater. Chem.*, **20** (37), pp. 7906-7915 (2010).

19. Ovid’Ko, I. “Enhanced mechanical properties of polymer-matrix nanocomposites reinforced by graphene inclusions: a review”, *Rev. Adv. Mater. Sci.*, **34** (1), pp. 19-25 (2013).

20. Zeng, Q., Yu, A. and Lu, G. “Multiscale modeling and simulation of polymer nanocomposites”, *Prog. Polym. Sci.*, **33** (2), pp. 191-269 (2008).

21. Rissanou, A.N. and Harmandaris, V. “Structure and dynamics of poly (methyl methacrylate)/graphene systems through atomistic molecular dynamics simulations”, *J. Nanopart. Res.*, **15** (5), pp. 1589 (2013).

22. Rissanou, A.N. and Harmandaris, V. “Dynamics of various polymer–graphene interfacial systems through atomistic molecular dynamics simulations”, *Soft Matter.*, **10** (16), pp. 2876-2888 (2014).

23. Alian, A., Dewapriya, M. and Meguid, S., "Molecular dynamics study of the reinforcement effect of graphene in multilayered polymer nanocomposites", *Mater. Design*, **124**, pp. 47-57 (2017).

24. Güryel, S., Walker, M., Geerlings, P., De Proft, F. and Wilson, M. "Molecular dynamics simulations of the structure and the morphology of graphene/polymer nanocomposites", *Phys. Chem. Chem. Phys.*, **19** (20), pp. 12959-12969 (2017)

25. Sun, R., Li, L., Feng, C., Kitipornchai, S. and Yang, J. "Tensile behavior of polymer nanocomposite reinforced with graphene containing defects", *Eur. Polym. J.*, **98**, pp. 475-482 (2018)

26. Skountzos, E.N., Anastassiou, A., Mavrantzas, V.G. and Theodorou, D.N. "Determination of the mechanical properties of a poly (methyl methacrylate) nanocomposite with functionalized graphene sheets through detailed atomistic simulations", *Macromolecules*, **47** (22), pp. 8072-8088 (2014).

27. Ebrahimi, S., Ghafoori-Tabrizi, K. and Rafii-Tabar, H. "Multi-scale computational modelling of the mechanical behaviour of the chitosan biological polymer embedded with graphene and carbon nanotube", Comp. Mater. Sci., **53** (1), pp. 347-353 (2012).

28. Rahman, R. and Haque, A. "Molecular modeling of crosslinked graphene–epoxy nanocomposites for characterization of elastic constants and interfacial properties", *Compos. Part B-Eng.*, **54**, pp. 353-364 (2013).

29. Theodorou, D.N. and Suter, U.W. "Atomistic modeling of mechanical properties of polymeric glasses", *Macromolecules*, **19** (1), pp. 139-154 (1986).

30. Rapold, R.F., Suter, U.W. and Theodorou, D.N. “Static atomistic modelling of the structure and ring dynamics of bulk amorphous polystyrene”, *Macromol. Theory Simul.,* **3** (1), pp. 19-43 (1994).

31. Theodorou, D.N. and Suter, U.W. “Detailed molecular structure of a vinyl polymer glass” *Macromolecules*, **18** (7), pp. 1467-1478 (1985).

32. Zhang, J., Chan-Park, M.B. and Li, C.M. “Network properties and acid degradability of epoxy-based SU-8 resists containing reactive gamma-butyrolactone”, *Sensor. Actuat. B-Chem.*, **131** (2), pp. 609-620 (2008).

33. Majidian, M., Grimaldi, C., Pisoni, A., Forró, L. and Magrez, A. “Electrical conduction of photo-patternable SU8–graphene composites”, *Carbon*, **80, pp.** 364-372 (2014).

34. Liu, Y., Zhang, C., Du, Z. and Li, H. “Preparation and curing kinetics of bisphenol A type novolac epoxy resins”, *J. Appl. Polym. Sci.*, **99** (3), pp. 858-868 (2006).

35. Tam, L-h. and Lau, D. “Moisture effect on the mechanical and interfacial properties of epoxy-bonded material system: An atomistic and experimental investigation”, *Polymer*, **57**, pp. 132-142 (2015).

36. Suter, M., Ergeneman, O., Zürcher, J., Moitzi, C., Pané, S., Rudin, T., Pratsinis, S., Nelson, B. and Hierold, C. “A photopatternable superparamagnetic nanocomposite: Material characterization and fabrication of microstructures”, *Sensor. Actuat. B-Chem.*, **156** (1), pp. 433-443 (2011)

37. Hossenlopp, J., Jiang, L., Cernosek, R. and Josse, F. “Characterization of epoxy resin (SU-8) film using thickness-shear mode (TSM) resonator under various conditions”, *J. Polym. Sci. Pol. Phys.*, **42** (12), pp. 2373-2384 (2004).

38. Tam, L-h. and Lau, D., ”A molecular dynamics investigation on the cross-linking and physical properties of epoxy-based materials", *RSC Adv.*, **4** (62), pp. 33074-33081 (2014).

39. Shuichi, N. “Constant temperature molecular dynamics methods”, *Prog. Theor. Phys. Supp.*, **103**, pp. 1-46 (1991).

40. Hoover, W.G., “Constant-pressure equations of motion”, *Phys. Rev. A.*, **34** (3), pp. 2499-2500 (1986).

41. Verlet, L. “Computer" experiments" on classical fluids. I. Thermodynamical properties of Lennard-Jones molecules”, *Phys. Rev.*, **159** (1), pp. 98-103 (1967).

42. Verlet, L. “Computer" experiments" on classical fluids. ii. equilibrium correlation functions”, *Phys. Rev.*, **165** (1), pp. 201-214 (1968).

43. Plimpton, S. Crozier, P. and Thompson, A. “LAMMPS-large-scale atomic/molecular massively parallel simulator”, *Sandia National Laboratories*, **18** (2007).

44. Lin, F., Xiang, Y. and Shen, H-S. “Temperature dependent mechanical properties of graphene reinforced polymer nanocomposites–A molecular dynamics simulation”, *Compos. Part B-Eng.*, **111,** pp**.** 261-269 (2017).

45. Ragab, T., McDonald, J. and Basaran, C. “Aspect ratio effect on shear modulus and ultimate shear strength of graphene nanoribbons”, *Diam. Relat. Mater.*, **74**, pp. 9-15 (2017).

46. Seitz, J. “The estimation of mechanical properties of polymers from molecular structure”, *J. Appl. Polym. Sci.* **49** (8), pp. 1331-1351 (1993).

Faraz Mohammadzadeh Honarvar is a last-year polymer engineering PhD student at Sahand University of Technology, Tabriz, Iran. He received a bachelor’s degree in Polymer Engineering Amirkabir University of Technology (Tehran Polytechnic), Tehran, Iran and a master’s degree in Polymer Engineering from University of Tehran, Tehran, Iran. His research fields are

nanocomposites, mechanical properties of nanocomposites and simulation of nanocomposites in molecular and macro scales. Also he is interested in multi-scale simulation.

Behzad Pourabbas received his Ph.D. in polymer Science and Technology from University of Shira, Shiraz, Iran, in 1996.
He joined the Department of Chemical Engineering at Sahand University of Technology in Tabriz, Iran, as an assistant professor in that year, the institution which he is still member of the faculty. He promoted to associate professor position in 2005 and to full professor position in 2009. In 2008 he when the department of Polymer Engineering has started its activity as an independent department, he joined the department and worked as the first head of the department.
During his academic career, he thought Physical Chemistry of Polymers, Polymer Physics, Polymer Characterization Methods and Organic Chemistry.
His main research activities focus on Nanostructured Materials, Surface and Surface modification, Nano-microfabrication, Conducting polymers and Electronic Materials. His is now Research Vice-Chancellor of the University since 2016.

Mahdi Salami Hosseini got his BSc and MSc degree from Amirkabir University of Technology in 2001 and 2004, respectively. He received his PhD from Amirkabir University of Technology in polymer engineering, 2009. He joined Polymer Engineering Department at Sahand University of Tecnology as assistant professor in 2009 and became associate professor in 2015. His current research interests include process simulation and numerical rheology using Finite Element Method (FEM) and Stokesian Dynamics (SD) focusing on microfluidic devices.

Mahsa Kharazi received her Ph.D. degree in Aerospace Engineering from Amirkabir University of Technology (Tehran Polytechnic) Tehran, Iran, in 2008.
In 2008 she joined the Department of Mechanical Engineering, Sahand University of Technology in Tabriz, Iran, as an assistant professor. Since then she has been a faculty member of the Mechanical Engineering Department at Sahand University of Technology and she became an associate professor in 2017.

Her teaching areas are Continuum Mechanics, Plasticity, Finite Element Method and Stability of Structures. Her Ph.D. thesis was on the stability analysis of delaminated composite materials and over the last five years she has become involved in damage modeling and analysis in solid mechanics. Her current research interests include Strutural Satability, Damage Analysis, Numerical Methods and Non-Local Theories.

Hamid Erfan-Niya received the PhD degree in Chemical Engineering, in 2011, from Amirkabir University of Technology (Tehran Polytechnic), Tehran, Iran. He is currently assistant professor of Chemical Engineering at University of Tabriz, Tabriz, Iran. His research interests are molecular simulation of nanoscale phenomena. Also, he works on interfacial phenomena, membrane-based water desalination, and gas separation systems. His published articles are related to the subjects including gas hydrates, nanofluids, nanocomposites, water desalination, and drug delivery systems.

Table of abbreviations

Table 1 Detailed explanation of the simulation strategy of the simulated SU8 and its graphene nanocomposites

Table 2 Calculated density for the simulated systems at 298 °K

Table 3 Calculated square end-to-end distance R^2 and average radius of gyration R_g for the model SU8 molecules in different systems

Table 4 Normalized mechanical properties (Young, shear and bulk modulus) for the model SU8 and its nanocomposites

Fig. 1 The representative model SU8 (a and b), a high aspect ratio graphene (26.18 A□ × 13.337 A□) (b) a low aspect ratio graphene (19.638 A□ × 14.546 A□) (c). Carbon, hydrogen and oxygen atoms are demonstrated by gray, white and red colored spheres, respectively

Fig. 2 Snapshot of a typical nanocomposite simulation cell involving 50 model SU8 and two graphene layers (4.2 wt.%). Graphene layers are indicated by blue but gray, white and red colored spheres are carbon, hydrogen and oxygen (in SU8), respectively

Fig. 3 Radius of gyration (R_g) versus probability density for the model SU8 in the simulated systems

Fig. 4 Intermolecular radial distribution function (RDF) for the paired atoms in the simulated systems: SU8, SU8GL21, SU8GL42, SU8GH21 and SU8GH42

Fig. 5 Intramolecular radial distribution function (RDF) for the paired atoms in the simulated systems: SU8, SU8GL21, SU8GL42, SU8GH21, SU8GH42

Fig. 6 The relative atomic concentration planner profile along the three main simulation axis (001, 010, 001) for the nanocomposite containing 2.1 wt.% of GH or GL graphene

Fig. 7 Average Young modulus of the compounds normalized with respect to pure SU8

Fig. 8 Average bulk modulus of the compounds with respect to the pure SU8

Fig. 9 Average shear modulus of the compounds with respect to the pure SU8

Figures and Tables

Table of abbreviations

Symbol	Description
U	Internal Energy
C_{ij}	Elastic Constants
σ	Stress
$\boldsymbol{\varepsilon}$	Strain
λ, μ	Lame's constants
E	Young's Modulus
B	Bulk Modulus
G	Shear Modulus
V	Volume
P	Pressure
P	Density
T	Temperature
B	Compressibility

Table 1

Notation	Number of the model SU8	Type of graphene	Number of graphene	Graphene

			layers	wt. %
SU8	50	-	-	-
SU8-GL21	50	Low aspect ratio	1	2.1%
SU8-GL42	50	Low aspect ratio	2	4.2%
SU8-GH21	50	High aspect ratio	1	2.1%
SU8-GH42	50	High aspect ratio	2	4.2%

Table 2

System	Predicted density (g/cm^3)	Experimental and/or theoritical values (g/cm^3)
SU8	1.088± 0.002	1.05 to 1.19 [35-37]
SU8-GH21	1.097± 0.004	N.A.
SU8-GH42	1.096± 0.003	N.A.
SU8-GL21	1.023± 0.005	N.A.
SU8-GL42	1.021± 0.003	N.A.

Table 3

System	R^2 (Å^2)	Average radius of gyration R_g (Å)
SU8	208.17	10.42
SU8-GH21	176.18	8.81
SU8-GH42	180.28	9.01
SU8-GL21	193.97	9.70
SU8-GL42	186.11	9.31

Table 4

Sample	**Normalized Value**		
	Young Modulus	**Bulk Modulus**	**Shear Modulus**
SU8	1.000 ± 0.039	1.00 ± 0.010	1.000 ± 0.013
SU8-GH21	1.631 ± 0.075	2.017 ± 0.012	1.820 ± 0.020
SU8-GH42	1.807 ± 0.075	2.165 ± 0.018	1.832 ± 0.014
SU8-GL21	1.169 ± 0.076	1.283 ± 0.026	1.160 ± 0.028
SU8-GL42	1.361 ± 0.081	1.591 ± 0.015	1.483 ± 0.015

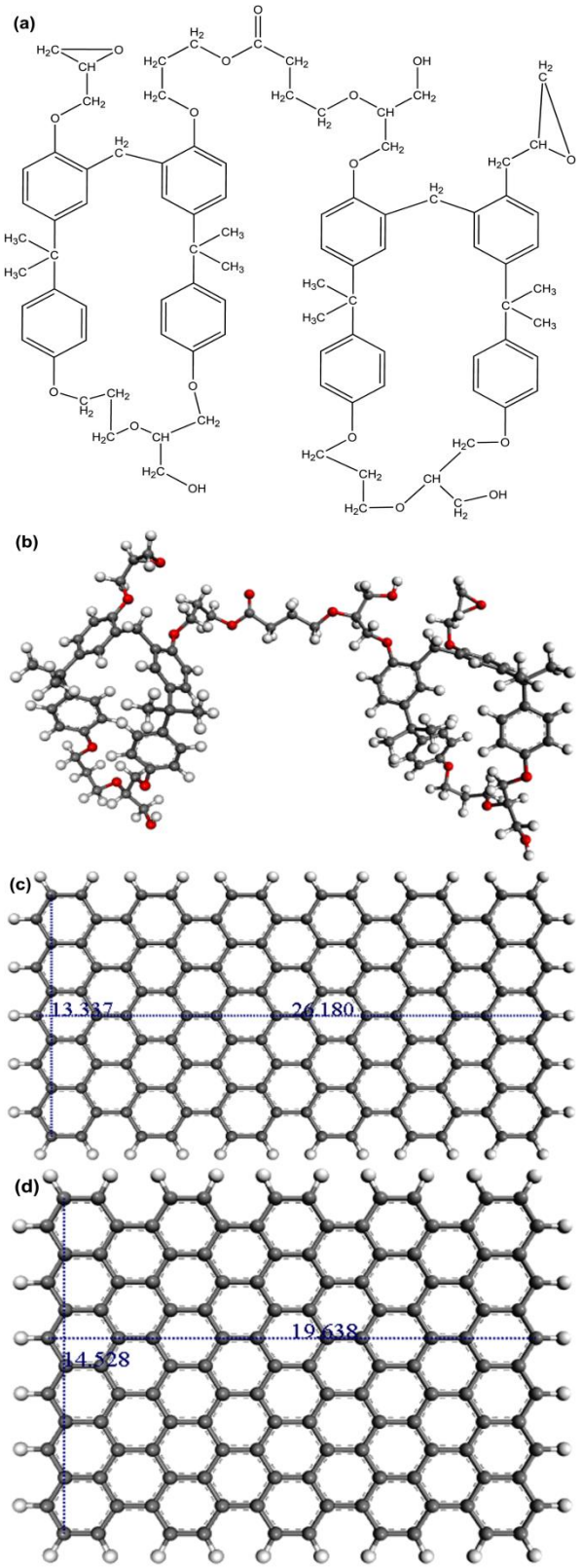

Fig 1

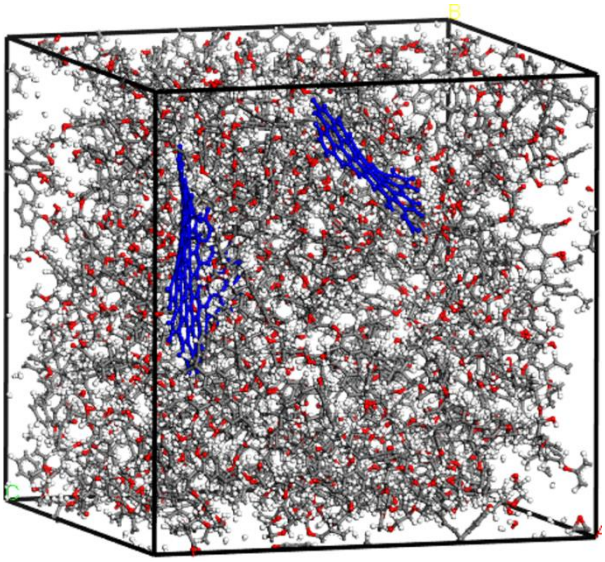

Fig 2

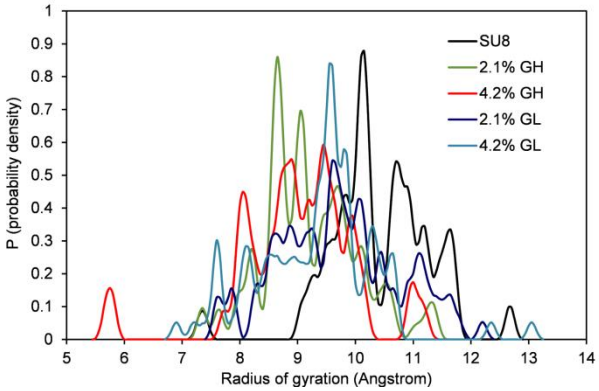
SU8
2.1% GH
4.2% GH
2.1% GL
4.2% GL
P (probability density)
Radius of gyration (Angstrom)
0
0.1
0.2
0.3
0.4
0.5
0.6
0.7
0.8
0.9
1
5
6
7
8
9
10
11
12
13
14

Fig 3

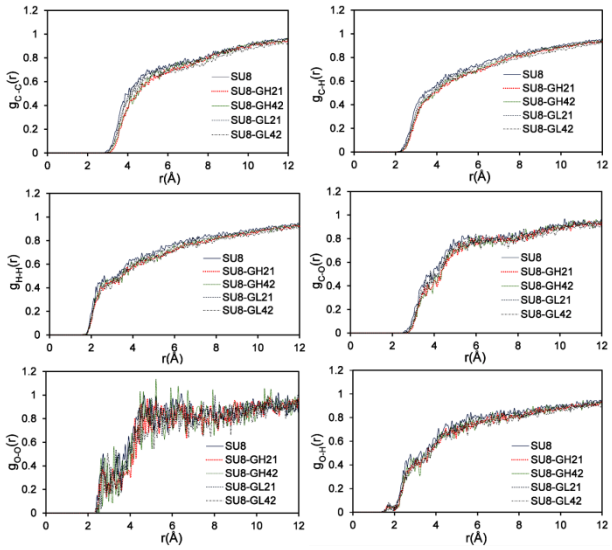
$g_{C\text{-}C}(r)$
$g_{C\text{-}H}(r)$
$g_{H\text{-}H}(r)$
$g_{C\text{-}O}(r)$
$g_{O\text{-}O}(r)$
$g_{O\text{-}H}(r)$
r(Å)
SU8
SU8-GH21
SU8-GH42
SU8-GL21
SU8-GL42

Fig 4

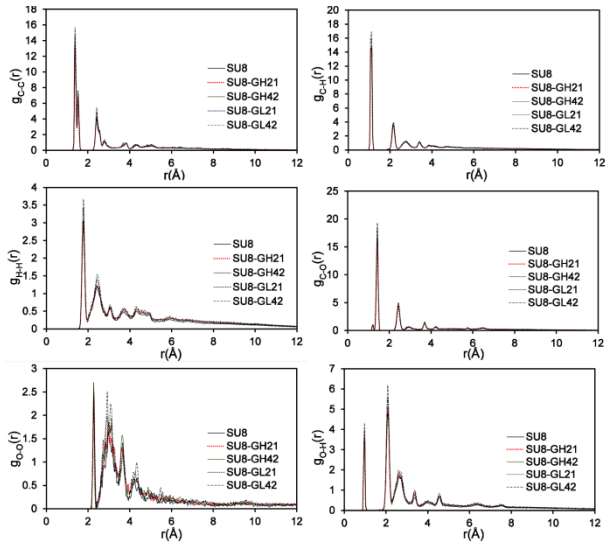
$g_{C\text{-}C}(r)$
$g_{C\text{-}H}(r)$
$g_{H\text{-}H}(r)$
$g_{C\text{-}O}(r)$
$g_{O\text{-}O}(r)$
$g_{O\text{-}H}(r)$
r(Å)
SU8
SU8-GH21
SU8-GH42
SU8-GL21
SU8-GL42

Fig 5

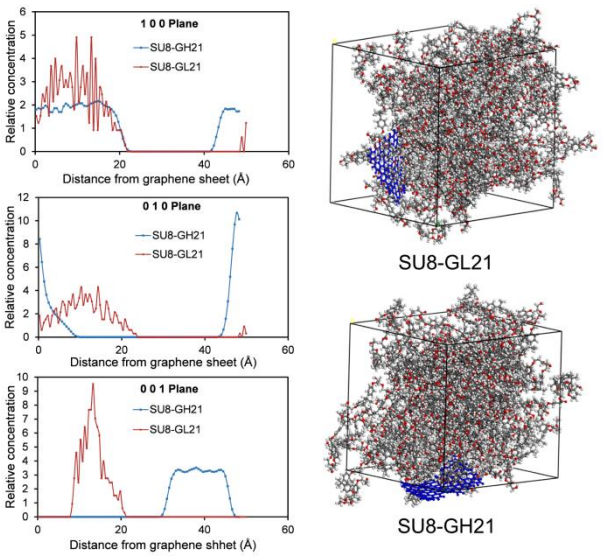

Fig 6

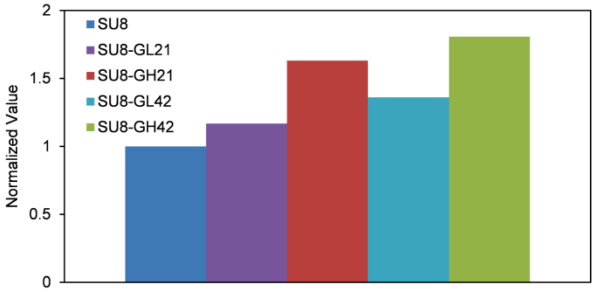

Fig 7

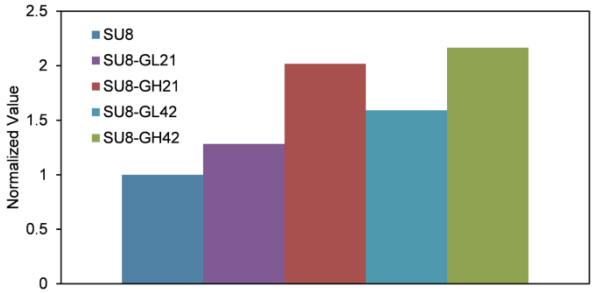

Fig 8

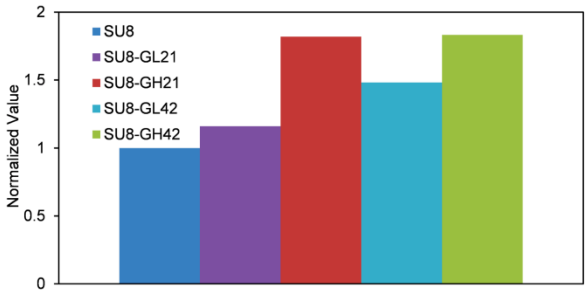
2
1.5
1
0.5
0
Normalized Value
SU8
SU8-GL21
SU8-GH21
SU8-GL42
SU8-GH42

Fig 9